




## Article

# Amantadine-Heparin-Polypyrrole as a Promising Drug Delivery Reservoir with a Biological Approach

Sara Kulik <sup>1,\*</sup> , Sylwia Golba <sup>2,\*</sup> , Izabela Matuła <sup>2</sup>, Ewa Stodolak-Zych <sup>3</sup>  and Roksana Kurpanik <sup>3</sup>

<sup>1</sup> Doctoral School, Department of Science and Technology, Institute of Materials Engineering, University of Silesia, Bankowa 14, 40-007 Katowice, Poland

<sup>2</sup> Department of Science and Technology, Institute of Materials Engineering, University of Silesia, Bankowa 14, 40-007 Katowice, Poland; izabela.matula@us.edu.pl

<sup>3</sup> Department of Biomaterials and Composites, Faculty of Materials Science and Ceramics, AGH University of Science and Technology, 30-059 Cracow, Poland; stodolak@agh.edu.pl (E.S.-Z.); kurpanik@agh.edu.pl (R.K.)

\* Correspondence: sara.krawczyk@us.edu.pl (S.K.); sylwia.golba@us.edu.pl (S.G.); Tel.: +48-666-847-133 (S.K.)

**Abstract:** There is an urgent need to alleviate the symptoms of neurodegenerative diseases. The presented work includes the use of electrochemical polymerization (CV) to obtain active polypyrrole layers with incorporated molecules of a neurological drug substance—amantadine hydrochloride. The obtained films were characterized chemically, structurally, and functionally in terms of their use as a drug delivery systems which are neurologically active. FTIR spectra were recorded to identify the incorporation of drug substances into the matrix. The obtained results showed that amantadine and heparin were embedded to the polypyrrole matrix. Scanning electron microscopy (SEM) was used to examine the morphology of the films. The films deposited on the steel substrate showed a compact, smooth structure, where there was no visible organized structure. After release, the film became corrugated. Adhesive tests were conducted with the cross-cut Test Method B to determine the mechanical properties, and the results showed that amantadine improves adhesion for steel substrates. The films were potentially stimulated by chronoamperometry, and UV-Vis spectra were registered to calculate the concentration of AMA in the solution after release. The release curves indicate a 95% efficiency of AMA release over the studied time period and protocol. Later, antibacterial properties were tested. The proposed system was able to provide a daily dose of drugs that ensures a therapeutic effect. This is a significant step towards developing systems capable of delivering a wider range of doses, potentially in line with the full spectrum recommended for therapeutic efficacy. The antibacterial properties of the material allows it to be considered as a material with antibacterial potential in the presence of the *Staphylococcus aureus* (*S. aureus*) strain. The percentage reduction ratio indicates a 90–100% reduction of bacteria in the suspension.

**Keywords:** conducting polymers; amantadine hydrochloride; polypyrrole; antibacterial test; neurologically active system



**Citation:** Kulik, S.; Golba, S.; Matuła, I.; Stodolak-Zych, E.; Kurpanik, R. Amantadine-Heparin-Polypyrrole as a Promising Drug Delivery Reservoir with a Biological Approach. *Coatings* **2024**, *14*, 1389. <https://doi.org/10.3390/coatings14111389>

Academic Editors: Lavinia Cosmina Ardelean and Laura-Cristina Rusu

Received: 9 October 2024

Revised: 28 October 2024

Accepted: 29 October 2024

Published: 31 October 2024



**Copyright:** © 2024 by the authors. Licensee MDPI, Basel, Switzerland. This article is an open access article distributed under the terms and conditions of the Creative Commons Attribution (CC BY) license (<https://creativecommons.org/licenses/by/4.0/>).

## 1. Introduction

Current demographic trends indicate that society is aging. Statistics from the World Health Organization (WHO) and the United Nations (UN) show that the population of people of elderly age affected by neurodegeneration diseases will increase from less than 1 million in 2020 to 2 million in 2050 [1,2]. Forecasts also indicate that the number of elderly people will be 1.5 billion in 2050, which is twice as many as in 2020 [3]. These changes also result in an increase in the incidence of dementia [4]. Dementia is a neurodegenerative disease that usually begins with a deterioration of cognitive functions—i.e., a deterioration of memory and thinking skills [5].

Neurodegenerative disorders are characterized by the progressive loss of selectively sensitive populations of neurons. The most common neurodegenerative disorders are amyloidoses (insoluble fibrous proteins that have specific structural features that allow them to

bind to specific dyes such as Congo red [6,7]) and tauopathies (tau protein associated with microtubules). The protein abnormalities in these disorders have abnormal conformational structures. Although neurodegenerative diseases are usually defined by specific protein accumulations and anatomical sensitivity, there are many underlying processes involved in progressive neuronal dysfunction and death [8], such as oxidative stress, programmed cell death, and neuroinflammation.

Alzheimer's disease is treated with two classes of drugs: cholinesterase inhibitors and glutamate regulators. Cholinesterase inhibitors work by inhibiting the breakdown of the neurotransmitter acetylcholine. Their side effects include vomiting, loss of appetite, nausea, and increased bowel movements. The only approved drug that regulates glutamate levels is the active substance memantine that is used to treat Alzheimer's disease (AD), which is associated with memory and learning. The drug's effectiveness is comparable to that of cholinesterase inhibitors, in that it works in about half of the people who take it and only for a short time [9]. Amantadine (AMA), an aminoadamantane long known for its moderate anti-Parkinsonian effects, has recently been shown to antagonize central N-methyl-D-aspartate (NMDA) receptors at therapeutically relevant concentrations.

A drug delivery system (DDS) is defined as a preparation or device that allows the introduction of a drug substance into the body and improves its efficacy and safety by controlling the rate, time, and location of drug release in the body. This process involves the administration of a drug product, the release of active ingredients by the product, and the subsequent transport of the active ingredients across biological membranes to the site of action. The term therapeutic substance also refers to an agent such as gene therapy that induces the production of an active therapeutic agent in vivo. A drug delivery system is the interface between a patient and a drug. It may be a form of drug to be administered for therapeutic purposes or a device used to administer the substance [10]. One of the most known materials used in DDS are conducting polymers.

Conducting polymers (CP) undergo a reversible redox reaction that causes ions to be transported into and out of the polymer. Typically, depending on the environmental conditions, a potential difference of less than 1 V must be applied to the electrode to release or capture ions. Conducting polymers can operate over a wide temperature range in a liquid electrolyte or in air using a polymer electrolyte [11]. It is assumed in the literature that polypyrrole (PPy), polythiophene (PTh), polyaniline (PANI), and their derivatives exhibit some biocompatibility with living tissues and body fluids. Long-term (90 days) in vitro and in vivo tests have shown little evidence of toxicity or immunological problems [12,13]. In the dedoped state, counterions are removed from the film and cause it to shrink. These properties can be exploited in drug delivery systems where drugs are incorporated into the polymer coating during oxidation and released during film reduction [14]. It is also possible to incorporate a cationic drug after the polymerization process, but the polymer must be doped with anions such as polystyrene sulfonate (PSS). During reduction of the polymer, the cationic drug is introduced to compensate for the negatively charged anions that cause the polymer to swell. During oxidation of the film, the cationic drug contained in it is released, and the film shrinks [15]. Cycles of film activation between redox states can cause cracks and discontinuities in the film, which can lead to an increased release rate of molecules [16]. Anionic drugs can also be introduced after the polymerization process by doping the polymer with a small anion, which can be the active form of the drug. Under these conditions, the coating oxidizes by incorporating anions and is reduced by releasing anions. In the case of introducing a relatively less mobile ion as a doping agent, both cationic and anionic drugs are simultaneously incorporated and removed [17].

PPy films loaded with anionic drugs (dexamethasone phosphate (DMP); meropenem (MER)) were deposited on the surface of indium tin oxide (ITO)-coated glass electrodes by electropolymerization by Shah et al. [18]. As a result of electrochemical oxidation (at a potential of 1 V) and polymerization of pyrrole on the anode, a layer was obtained. In the polypyrrole layer, the cationic charges were compensated with anionic dopants from the electrolyte (in this case, one of the anionic drugs—DMP or MER). The successful

deposition of polypyrrole films on the surface of ITO electrodes was noticeable (i.e., the presence of a black film on the surface of the transparent and colorless ITO electrode). It was observed that the release of relevant drugs (DMP or MER) loaded into PPy films was enhanced upon the application of electrochemical stimulus, providing proof of concept that such materials can form a useful protective coating on the surface of implantable medical devices, potentially reducing adverse reactions to their implantation in vivo [19]. Among the conductive polymers, the self-healing hydrogels were revealed [20]. Electrical conductivity was achieved by the polypyrrole, free ions, and the synergistic effect between the PPy particles and the free ions. The resultant hydrogels have potential applications in electronic skin and biomedical implants. These hydrogels improve mechanical properties such as toughness and stretchability [21].

The presented work includes the use of electrochemical polymerization (using two synthetic protocols) to obtain active polypyrrole layers with incorporated molecules of a neurological drug substance—amantadine hydrochloride. To our knowledge and review of source materials in the literature, there is no yet known amantadine-loaded polypyrrole coating. The obtained layers will be characterized in terms of their use as drug delivery systems neurologically active which is used in medicine. The developed procedure for deposition of the amantadine-enriched coating allows for the control of the mass and morphology of the deposited polymer, which directly affects the amount of encapsulated drug. The proposed system can be prepared on various conductive substrates (e.g., medical steel, platinum), which expands the solution's applicability. Optimal electrochemical synthesis conditions were developed to obtain coatings with high drug accumulation capacity and very good adhesion to the substrate (class 4B according to ASTM D3359-23, Standard Test Methods for Rating Adhesion by Tape Test, World Trade Organization Technical Barriers to Trade (TBT) Committee, New York, 2023). The process of amantadine release is confirmed and potential controlled, allowing for the control of the release rate.

## 2. Materials and Methods

### 2.1. Synthesis

The synthesis was performed in an aqueous medium containing the following ingredients: pyrrole (98%, Sigma Aldrich, Schnelldorf, Germany), amantadine hydrochloride AMA (>98% TLC, Sigma Aldrich, Schnelldorf, Germany), and necessary commercially available heparin sodium salt from porcine intestinal mucosa (HEP) (>180 USP units/mg, Sigma Aldrich, Schnelldorf, Germany) and sodium dodecyl sulphate (>99% Sigma Aldrich, Schnelldorf, Germany). Prior to synthesis, pyrrole was pre-distilled for purification, resulting in a transparent pale yellow liquid, which was then stored in a freezer. The electrolyte solution was prepared by dissolving SDS in distilled water to achieve a concentration of 0.1 M, surpassing the critical micelle concentration of 0.008 M [22]. The monomer solution was prepared at a concentration of 0.2 M with the molar ratio of the components AMA:HEP:Py set at 1:0.005:2. To avoid inhomogeneities, the synthetic solution was freshly prepared just before the experiment. The stainless steel substrate (316L (Stalglass)) was used due to its relevance for biomedical applications (composition: Cr 16%, Ni 10%, Mo 2%, C 0.08%, P 0.045%, S 0.03%, Si 0.75%, N 0.1%). Stainless steel (square, 8 mm × 8 mm) was used as a working electrode (WE) prepared by polishing with sandpaper (ranging from grit 300 to 600 Klingspor, Bielsko Biała, Poland) and washed with distilled water to remove any powder impurities. Subsequently, the substrate was immediately immersed in a 60% ethanol solution for 24 h to prevent the formation of an oxide layer. All measurements were conducted at room temperature. Indium tin oxide-coated PET (60 Ω/sq, 5 mil) (Sigma Aldrich, Schnelldorf, Germany) was immersed in distilled water and acetone before usage.

### 2.2. Polymerization of AMA/HEP/Py via CV and CR Methods: Procedures Used to Stimulate the Release of Entrapped AMA and HEP

The measurements were carried out in an electrochemical cell containing a reference Ag/AgCl electrode, a counter electrode (platinum spiral), and a 316 L steel plate or ITO

as a working electrode. Cyclic voltammetry (CV) was employed for the synthesis and characterization of the deposited polymeric films. The CV analysis was performed using an Autolab PGSTAT12 potentiostat, and the results were analyzed with Autolab software (version 4.9). During the synthesis, two maximum potentials were applied,  $E = 0.70$  V and  $E = 0.85$  V, with different numbers of cycles (20 cycles and 30 cycles) to detect their influence on the deposition process as well as on drug immobilization efficiency. To stimulate the release of the drug substance, chronoamperometry was used with a potential set at either 0.5 or 0.7 V, held for 150 s, and in long term release for 48 h. The scheme of the releasing procedure is shown in Figure 1.

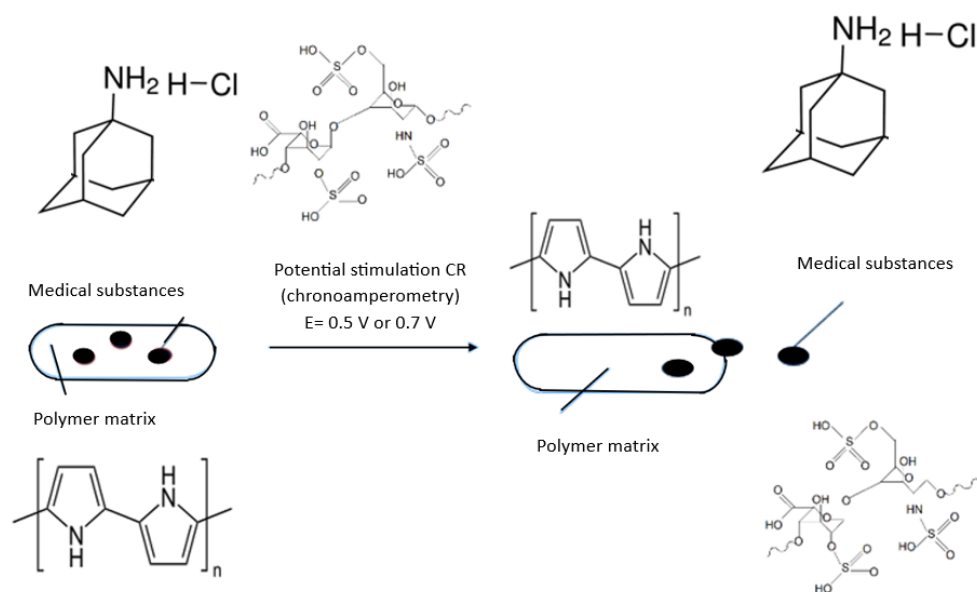


**Figure 1.** Scheme of potential release of AMA and HEP from PPy matrix.

### 2.3. Characterization of AMA/HEP/PPy Films

Scanning electron microscopy (SEM) was carried out using a Hitachi S4100 microscope equipped with an energy-dispersive X-ray spectrometer (EDS) with an acceleration voltage of 15 keV. For these analyses, the samples were firmly fixed onto a steel sample holder using adhesive carbon tape (SEM Conductive Double sided Carbon Tape, Extra Pure, width: 5 mm, micro-shop). Additionally, the surface of the PPy film was coated with an additional layer of carbon powder using an EMITECH K950X carbon coater to guarantee a conducting surface for the analysis.

The UV-Vis measurements were carried out using a quartz cuvette (Bionovo, Chorzów, Poland) in a Biowave II UV-vis spectrometer (WPA, Biochron, Surrey, UK). For the release stage, the coated samples were fully immersed in a 0.9% NaCl solution and placed along the side wall of the cuvette to allow the diffusion of drug molecules into the bulk of the solution. Aliquots of the solution were taken with a pipette (2.5 mL) and then poured into a measuring cuvette and placed in the UV-Vis spectrometer. The solution was then led back to the measuring cell, allowing simultaneous mixing of the solution. The absorption band of AMA was located at 237 nm [23], while the HEP absorption band was observed at 213 nm [24]. The spectra were recorded in real time with readings taken every 15 s, while a constant potential was applied using the AUTOLAB PGSTAT12 potentiostat. The chosen potentials values were based on the respective potentials observed in the CV doping/dedoping cycles. The system worked in air-conditioned room temperature.

### 2.4. Antimicrobial Activity of AMA/HEP/PPy Films

The biological properties of AMA/HEP/PPy film were tested on the basis of the PN-EN ISO 22196:2007 standard (Measurement of antibacterial activity on plastics and

other non-porous surfaces, Technical Committee ISO/TC 61, Plastics, Subcommittee SC 6, Ageing, chemical and environmental resistance, UK, 2011).

Preparation of strains *Escherichia coli* ATCC 8739 and *Staphylococcus aureus* ATCC 6538P: bacterial cultures were refreshed twice before analysis by sieving onto slants with nutrient agar and incubated for 24 h at  $35\text{ }^{\circ}\text{C} \pm 1\text{ }^{\circ}\text{C}$ .

Preparing materials for tests: The test and control materials were sterilized with 70% ethyl alcohol in an ultrasonic bath.

Inoculation: Microbial cells were suspended in a sterile nutrient broth with an amount of  $\sim 10^5$  cells/mL. The prepared test and control materials were placed in sterile Petri dishes. A dose of inoculum was applied to the surface of each plant and placed in a culture well.

Incubation: Sterile bags containing inoculated test materials and control materials were incubated for 24 h at  $35\text{ }^{\circ}\text{C} \pm 0.1\text{ }^{\circ}\text{C}$ .

According to the standard PN-EN ISO 22196:2007, the crucial R parameter can be calculated according to the Equation (1). The results give information on whether a material shows microbiological activity.

$$R = (U_t - U_0) - (A_t - U_0) = U_t - A_t \quad (1)$$

where:

$R$ —value of antimicrobial activity,

$U_0$ —average of the decimal logarithm of the number of live bacterial cells on control samples immediately after inoculation,

$U_t$ —average of the decimal logarithm of the number of live bacterial cells on control samples after 24 h of incubation,

$A_t$ —the average of the decimal logarithm of the number of live bacterial cells on samples tested after 24 h of incubation.

In turn, the percentage value of antimicrobial activity is expressed as Equation (2):

$$R[\%] = \frac{A - B}{A} \cdot 100 \quad (2)$$

where:

$R$ —percentage of antimicrobial activity,

$A$ —initial number of bacteria in the suspension contacted with the tested materials, CFU,

$B$ —number of bacteria after 24 h of contact between bacteria and the tested material, CFU.

### 3. Results

#### 3.1. Synthesis and Electrochemical Characterization of AMA/HEP/PPy

PPy was synthesized in the presence of amantadine (AMA) and heparin (HEP) using cyclic voltammetry in a sodium dodecyl sulfate solution. The aim of this study is to prepare a system with a portion of AMA enclosed in the polymer structure. The incorporation of saccharide-type HEP is dictated by its anionic character, which allowed it to serve as a polymeric counterion, balancing the positive charge generated during the growth of PPy chains. At the same time, large HEP molecules can be incorporated into the PPy matrix, interacting with AMA molecules (AMA is a cationic drug). Electropolymerization at a molar ratio of AMA/HEP/PPy 0.1:0.002:0.1 M was induced by cyclic voltammetry in a specify potential range. Two values of maximum potentials were defined:  $E_1 = 0.70\text{ V}$  and  $E_2 = 0.85\text{ V}$ . The process parameters are shown in the table below (Table 1). The samples were numbered, taking into account the process parameters and the used substrate.

**Table 1.** Electrochemical synthesis parameters of AMA/HEP/PPy.

Potential	N° Scan	Film	Substrate
$E_{1\max} = 0.70$ V	20	$f_1$	ITO
	30	$f_2$	
$E_{2\max} = 0.85$ V	20	$f_3$	
	30	$f_4$	
$E_{1\max} = 0.70$ V	20	$f_5$	Steel
	30	$f_6$	
$E_{2\max} = 0.85$ V	20	$f_7$	
	30	$f_8$	

An example of the cyclic voltammogram of AMA/HEP/PPy is shown in the figure (Figure 2). In order to characterize the deposition process of the AMA/HEP/PPy system, the CV cyclic voltammetry technique was used in the potential range from  $-0.45$  to  $0.85$  V and from  $-0.35$  to  $0.70$  V with respect to the Ag/AgCl electrode.

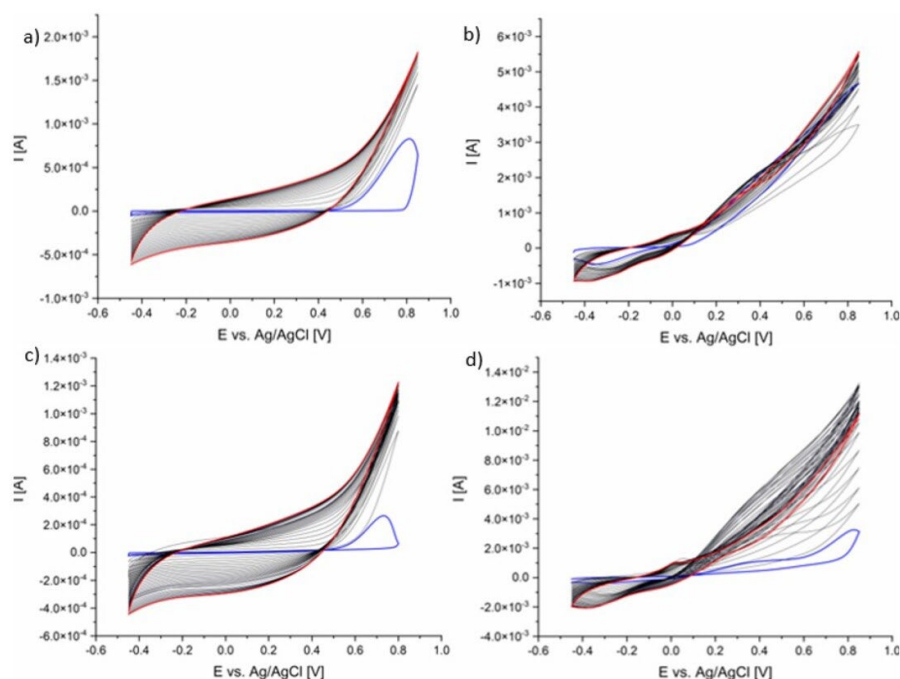


**Figure 2.** Cyclic voltammograms during synthesis of AMA/HEP/PPy films: (a)  $f_3$ ; (b)  $f_7$ ; (c)  $f_4$ ; (d)  $f_8$  (abbreviation explained in Table 1).

The CV curves during the synthesis (Figure 1) of the AMA/HEP/PPy system recorded at a potential of  $0.85$  V were significantly different in shape from the curves obtained at  $0.7$  V (Figure S1). The curves of the films on the ITO substrate showed a higher current amplitude. The CV curve corresponding to the polymerization process on the steel substrate showed higher current values by two orders of magnitude for  $f_7$  and by one order of magnitude for  $f_8$  compared to  $f_5$  and  $f_6$ . Oxidation peaks were visible at a potential of  $0.05$  V and reduction at  $-0.35$  V for  $f_7$  and  $f_8$ . The electropolymerization process was more balanced for the films on the ITO substrate. The process proceeded according to the scheme of pyrrole polymerization, where the monomer was oxidized, cation-radical coupling occurred, and less soluble chains were formed and grew, which adsorbed on the electrode surface. The electrochemical synthesis process on a steel substrate was less effective, but it produced a more electrochemically active film (doping and dedoping peaks were visible). The higher applied potentials led to intensive oxidation of the monomer, which did not undergo further effective polymerization. Hysteresis appeared on the CV

with each subsequent cycle (the cathodic current intensity was higher than the anodic current), which may indicate changes in the nature of the substrate during the process.

The ITO and steel electrodes were fully coated with AMA/HEP/PPy layers prepared according to the given procedures. To characterize the polypyrrole films, cyclic voltammograms of the obtained films were recorded in the SDS environment.

The CV curves of  $f_5$  and  $f_6$  films (Figure S2) do not overlap, and after each cycle, the curves change, which indicates low electrochemical stability. On the surface of the working electrode, intensive ion exchange occurs in the electrolyte solution [25]. The electrolyte solution became colored and turned turbid, which was caused by dissolution of oligomers and migration to the film, which can be observed as a decrease in current intensity. The CV curves (Figure 3) showed higher values of current intensity for all films, compared to the curves in the Figure S2. The widest amplitudes of the curves were visible for the films on the steel substrate, which indicates their charge storage ability. The curves for  $f_7$  and  $f_8$  overlap, indicating better electrochemical stability compared to  $f_5$  and  $f_6$ . The table (Table 2) summarizes the values of electrochemical stability and film thickness calculated according to the Equations (3) and (4).

$$S = \frac{Q_{10}^+}{Q_2^+} \cdot 100\% \quad (3)$$

where:

$Q_{10}^+$ —the charge of the last doping half cycle [C],

$Q_2^+$ —the charge of the second doping half cycle [C].

$$g = \frac{q_{pol} \cdot M_{mon}}{n \cdot F \cdot A_w \cdot \rho} \quad (4)$$

where:

$g$ —the thickness of the dry polymer film formed in the electropolymerization process, [cm],  
 $q_{pol}$ —the total charge of the polymerization process, expressed as the charge of the last polymerization cycle,

$M_{mon}$ —molar mass of monomer [ $\text{g} \cdot \text{mol}^{-1}$ ],

$n$ —the number of electrons involved in the oxidation of one monomer unit, (2.3 for pyrrole [23],

$F$ —Faraday's constant, ( $96.48 \text{ C} \cdot \text{mol}^{-1}$ );

$A_w$ —the surface of the working electrode covered with a polymer film, ( $\text{cm}^2$ ),

$\rho$ —approx. film density ( $1.48 \text{ g} \cdot \text{cm}^{-3}$ ) [26].

The increase in the potential window during synthesis and the number of cycles influenced the increase in the film thickness, especially for  $f_4$  by about 50%. Increasing the potential window during synthesis influenced as well the electrochemical stability of the obtained films on both substrates. Increasing the number of cycles for coatings on ITO substrate at the applied lower potential of 0.7 V resulted in a decrease in the value of film stability. In the case of coatings obtained at 0.85 V, the stability of the coatings increased. Compared to coatings obtained on ITO, on steel, an increase in the number of potential cycles resulted in a decrease in the stability of coatings for  $E = 0.7 \text{ V}$  and an increase in the stability of coatings at  $E = 0.85 \text{ V}$ . In the polymer formation process, both anions and electrons moved through the film. In the subsequent reduction, the electroneutrality was restored by pushing out anions or by incorporating cations from the electrolyte solution. After applying a positive potential, the neutral film was oxidized and anions were absorbed or cations were rejected. The redox activity of the polymer was regulated by the electron transfer reaction and mass transport process. The decrease in stability values upon potential reduction was related to the difficulty of mass transport or electron transfer.

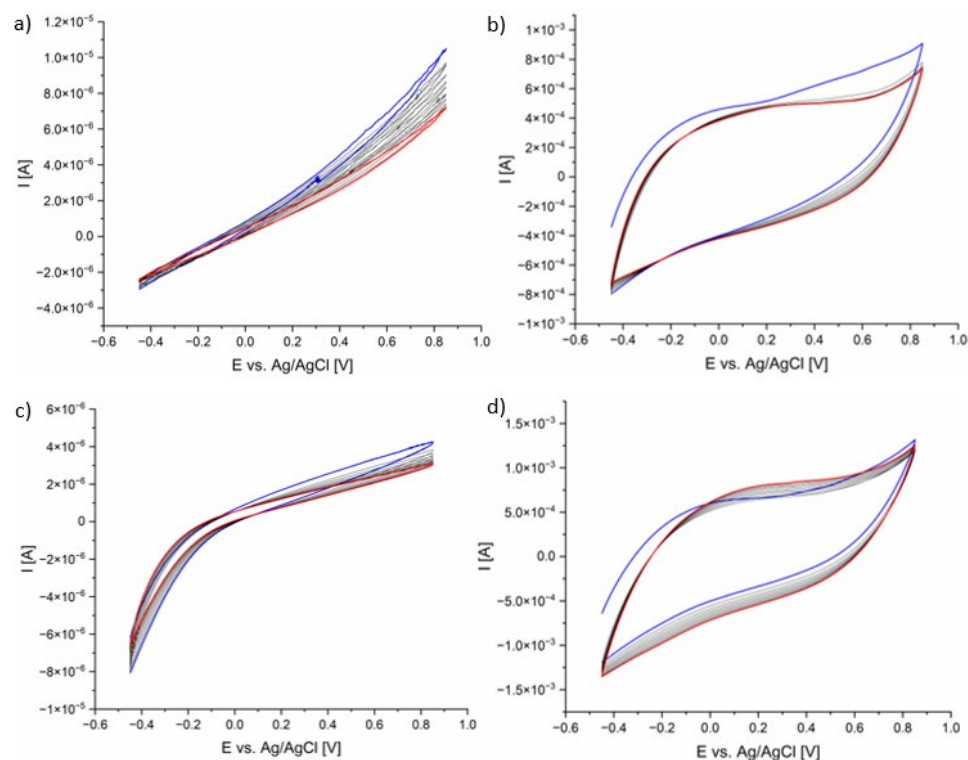


**Figure 3.** Cyclic voltammograms of AMA/HEP/PPy films: (a)  $f_3$ ; (b)  $f_7$ ; (c)  $f_4$ ; (d)  $f_8$  (abbreviation explained in Table 1).

**Table 2.** Electrochemical stability and thickness of AMA/HEP/PPy film deposited on ITO and steel substrates.

E = 0.70 V, c = 20			E = 0.70 V, c = 30		
Substrate	S [%]	g [ $\mu\text{m}$ ]	Substrate	S [%]	g [ $\mu\text{m}$ ]
ITO $f_1$	94.94	0.017	ITO $f_2$	75.84	0.019
Steel $f_5$	73.29	0.011	Steel $f_6$	61.41	0.12
E = 0.85 V, c = 20			E = 0.85 V, c = 30		
Substrate	S [%]	g [ $\mu\text{m}$ ]	Substrate	S [%]	g [ $\mu\text{m}$ ]
ITO $f_3$	71.70	0.036	ITO $f_4$	83.63	0.078
Steel $f_7$	93.80	0.13	Steel $f_8$	112.56	0.14

### 3.2. Morphology of AMA/HEP/PPy Films by SEM

Scanning electron microscopy was used to analyze the morphology of the deposited AMA/HEP/PPy films in pristine post-synthetic form and after the release event (results reported in the following section).

The films deposited on the steel substrate (Figure 4) showed a compact, smooth structure, where there was no visible organized structure. After release, the film became corrugated. Due to the potential release, the HEP molecules with high mass and AMA surface-bonded to PPy came out of the coating, hence the release voids were visible in the SEM image (marked with circles in Figure 3). Due to electrical stimulation, the drug substances bound by electrostatic interactions to oxidized PPy were released. In the case of the  $f_7$  film, after release, clusters were visible revealing a cauliflower-like structure (Figure S3), typical for PPy. The microstructures of the films on the steel substrate were different. During the synthesis, the micelle adsorption was less efficient, hence only trace amounts of the scaffold are visible, changing the structure to a more typical one (cauliflower-like).



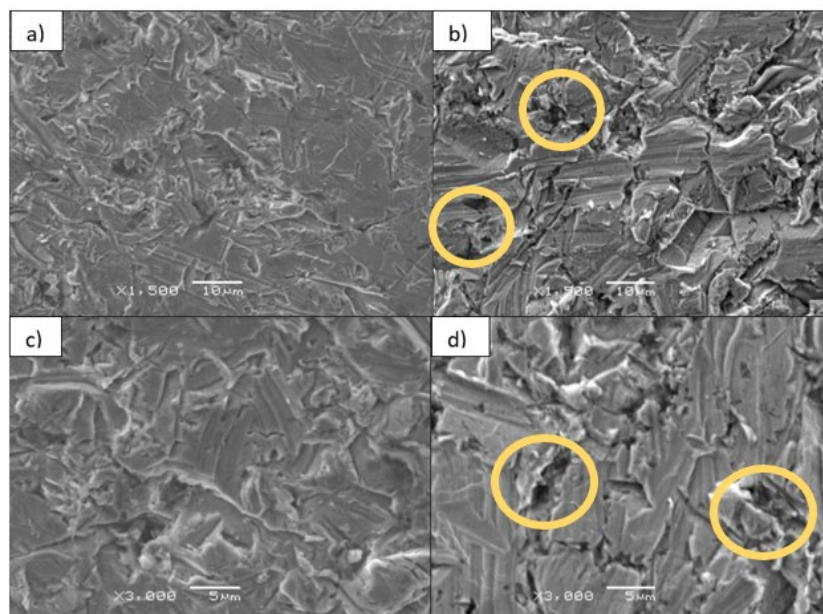


**Figure 4.** SEM images of the film  $f_5$  AMA/HEP/PPy on steel substrate: (a,c) before AMA and HEP release; (b,d) after 0.7 V potential release of AMA and HEP (voids after release of AMA and HEP marked with yellow circles).

### 3.3. Adhesion Tests of AMA/HEP/PPy Films

Adhesion tests were performed according to the ASTM D3359-23 standard. The investigation included Test Method B—cross-cut tape test. The test results of the obtained films were classified according to the requirements of the standard. The results are shown in the table (Table 3) and in the figure (Figure S4).

**Table 3.** Classification of AMA/HEP/PPy film adhesion test results according to ASTM D3359-23 standard (Standard Test Methods for Rating Adhesion by Tape Test, World Trade Organization Technical Barriers to Trade (TBT) Committee, New York, 2023).

Process Parameters	N° Scan	Film	Substrate	Classification
$E_{1max} = 0.70V$	20	$f_1$	ITO	0B
$E_{1max} = 0.70V$	30	$f_2$	ITO	2B
$E_{2max} = 0.85V$	20	$f_3$	ITO	1B
$E_{2max} = 0.85V$	30	$f_4$	ITO	0B
$E_{1max} = 0.70V$	20	$f_5$	Steel	3B
$E_{1max} = 0.70V$	30	$f_6$	Steel	2B
$E_{2max} = 0.85V$	20	$f_7$	Steel	4B
$E_{2max} = 0.85V$	30	$f_8$	Steel	1B

Based on the results, it is evidenced that AMA-added coatings improved the adhesion of the coating to the ITO substrate. The  $f_3$  film flaked along the edges of the cuts, the damaged area was within 60%, and the  $f_2$  coating was damaged within 35% of the grid. The results showed significantly better adhesion for the films on the steel substrate. The  $f_7$  film showed the best adhesion, with only small flakes peeling off at the line intersections (less than 5% of the area). The  $f_5$  coating peeled off within 15% of the cut grid area, and the  $f_6$  coating peeled off within 3%.

### 3.4. Short-Term Release of AMA and HEP from AMA/HEP/PPy Films

UV-Vis spectra (Figure 5) of solutions were recorded during the release of medicinal substances from AMA/HEP/PPy films. The initial spectrum was marked in blue, and then the next ones were recorded every 15 s. The spectrum after 150 s was marked in red.

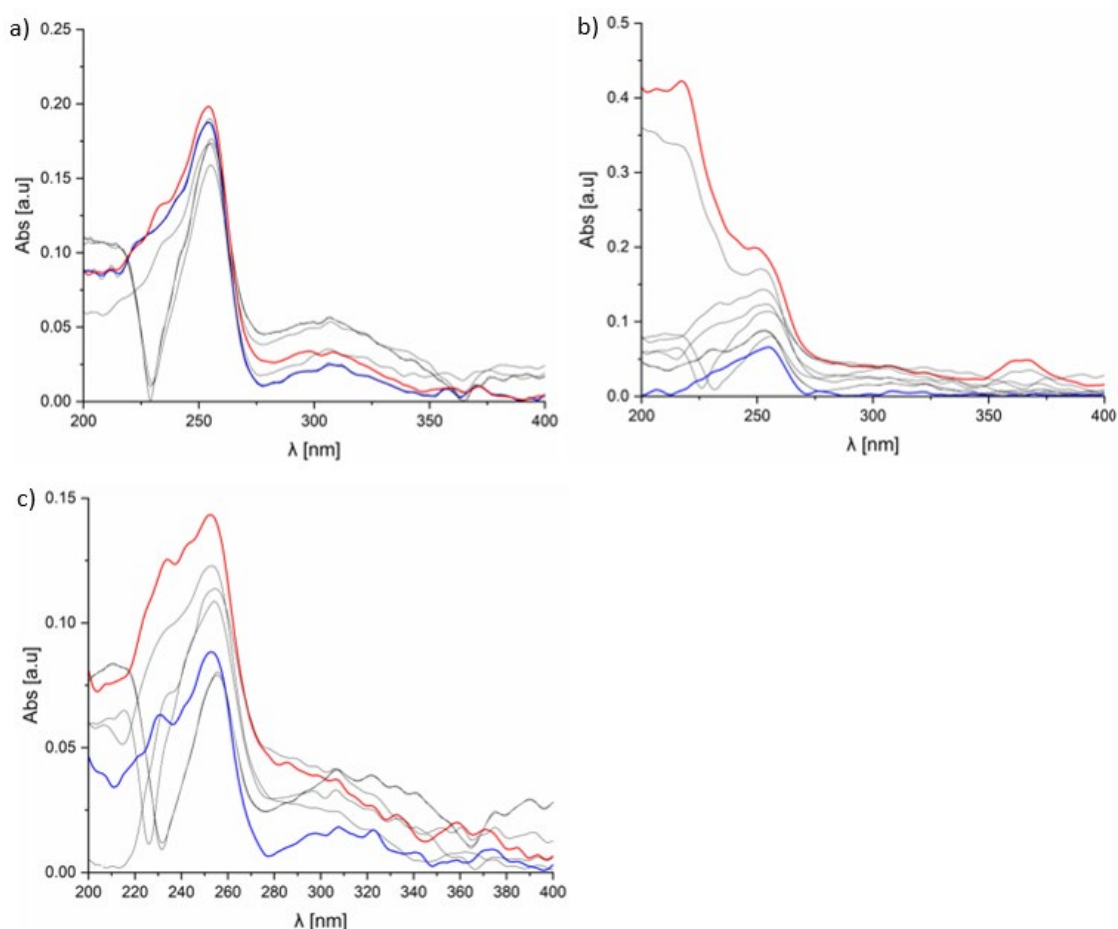


**Figure 5.** UV-Vis spectra during the release of AMA and HEP from the  $f_7$  AMA/HEP/PPy film: (a) at a constant potential of 0.5 V; (b) at a constant potential of 0.7 V; (c) diffuse.

Each spectrum showed characteristic bands corresponding to AMA  $\lambda = 269$  nm [26,27] and HEP  $\lambda = 213$  nm [28], and the absorbance values were converted to concentrations using absorption coefficients  $\epsilon = 3.9 \cdot 10^4 \text{ cm}^{-1} \cdot \text{M}^{-1}$  [29] for AMA and  $\epsilon = 5500 \text{ cm}^{-1} \cdot \text{M}^{-1}$  for HEP and are listed in the table below (Table 4). The absorbance value in the range of 200–220 nm is related to  $\pi\text{-}\pi^*$  electron transitions in C=C bonds or  $n\text{-}\pi^*$  from nitrogen atoms in amine groups. The highest concentrations of AMA were visible for solutions taken during desorption from the cell, in which the film was placed on a steel substrate. The HEP concentration values were six orders of magnitude lower compared to the AMA concentrations due to its lower molar fraction in the monomer solution and its high molecular weight.

The highest value of AMA concentration in solution was visible after the procedure of 0.7 V release from  $f_7$  film and the lowest for the procedure of diffusion release. It was observed that drug molecules were detached from the matrix more efficiently under the influence of higher potential. Drug concentration in solution after diffusion release showed one order of magnitude lower values compared to potential release. At the structural level, it could be concluded that during the oxidation reaction, the volume of the PPy matrix increased, which led to the release of the cationic drug (AMA) in a process called “cation-driven activation”. The expansion and increase in the volume of the polymer was controlled by changing the applied voltage. A higher value of the applied voltage caused intensification of the oxidation process, allowing for control over the release of drug molecules. This proved that the prepared AMA/HEP/PPy coatings were useful for the construction of drug delivery systems.

**Table 4.** List of concentrations of AMA and HEP after release from PPy matrix obtained from UV-Vis spectra.

Film	C for 0.5 V release [M]		C for 0.7 V release [M]		C for diffusion release [M]	
	HEP	AMA	HEP	AMA	HEP	AMA
f <sub>1</sub>	$9.09 \times 10^{-6}$	$8.46 \times 10^{-1}$	$1.82 \times 10^{-6}$	$1.77 \times 10^{-1}$	$3.64 \times 10^{-6}$	$6.15 \times 10^{-1}$
f <sub>2</sub>	$3.27 \times 10^{-5}$	$1.62 \times 10^1$	$5.82 \times 10^{-5}$	$2.23 \times 10^1$	$7.27 \times 10^{-6}$	$3.85 \times 10^{-1}$
f <sub>3</sub>	$9.09 \times 10^{-5}$	$1.92 \times 10^1$	$7.09 \times 10^{-5}$	$3.15 \times 10^1$	$1.09 \times 10^{-5}$	$6.92 \times 10^{-1}$
f <sub>4</sub>	$9.09 \times 10^{-6}$	$8.46 \times 10^{-1}$	$1.82 \times 10^{-5}$	$1.77 \times 10^1$	$3.64 \times 10^{-6}$	$6.15 \times 10^{-1}$
f <sub>5</sub>	$7.27 \times 10^{-5}$	$2.92 \times 10^1$	$6.55 \times 10^{-6}$	$7.69 \times 10^{-1}$	$1.09 \times 10^{-5}$	$1.54 \times 10^{-1}$
f <sub>6</sub>	$2.73 \times 10^{-5}$	$1.00 \times 10^1$	$8.36 \times 10^{-5}$	$1.85 \times 10^1$	$1.82 \times 10^{-5}$	$4.62 \times 10^{-1}$
f <sub>7</sub>	$2.36 \times 10^{-5}$	$2.00 \times 10^1$	$4.91 \times 10^{-5}$	$3.85 \times 10^1$	$1.64 \times 10^{-5}$	$8.46 \times 10^{-1}$
f <sub>8</sub>	$5.45 \times 10^{-5}$	$1.38 \times 10^1$	$5.82 \times 10^{-5}$	$2.77 \times 10^1$	$9.09 \times 10^{-6}$	$6.92 \times 10^{-1}$

Based on the obtained data from UV-Vis spectra, the release efficiency of the active substance (RE) was calculated. RE was calculated as the ratio of  $c_3$  to  $c_1$ , where  $c_3$  was the concentration of the substance in the solution after release, and  $c_1$  is the concentration of the active substance introduced into the matrix during synthesis. The value of  $c_1$  was calculated from the difference between the initial concentration of the active substance in the solution ( $c_0$ ) and its concentration after synthesis ( $c_2$ ). The values were converted to percentages. The table below (Table 5) also included the AMA encapsulation efficiency in polypyrrole films with the uncertainty calculated using the total differential, calculated on the basis of UV-Vis spectra data and Equation (5).

$$EE = \left[ \frac{\text{drug concentration in the polymer film}}{\text{drug concentration in the solution during synthesis}} \right] \cdot 100\% \quad (5)$$

**Table 5.** Release efficiency (RE) of AMA and HEP and encapsulation efficiency (EE) of AMA in polypyrrole films.

Film	AMA RE [%]	HEP RE [%]	AMA EE [%]	m AMA Released [mg·cm <sup>-3</sup> ]
f <sub>1</sub>	19.10 ± 0.25	8.90 ± 0.25	1.77 ± 0.11	1.79 ± 0.12
f <sub>2</sub>	28.44 ± 0.35	24.04 ± 0.32	22.30 ± 0.23	2.26 ± 0.16
f <sub>3</sub>	34.61 ± 0.41	33.96 ± 0.51	31.50 ± 0.28	3.19 ± 0.20
f <sub>4</sub>	30.12 ± 0.32	26.87 ± 0.28	17.70 ± 0.12	1.79 ± 0.17
f <sub>5</sub>	17.02 ± 0.32	12.08 ± 0.23	7.69 ± 0.09	1.84 ± 0.19
f <sub>6</sub>	25.11 ± 0.51	21.16 ± 0.42	18.50 ± 0.21	3.64 ± 0.26
f <sub>7</sub>	55.26 ± 1.10	47.24 ± 0.93	39.57 ± 0.31	5.13 ± 0.34
f <sub>8</sub>	39.36 ± 0.85	19.34 ± 0.14	27.70 ± 0.32	2.39 ± 0.21

The entrapment percentage for AMA was the highest for f<sub>7</sub> (39.5%) and for f<sub>3</sub> (31.5%) (Table 5), which was related to the higher roughness of the layers. The EE of AMA ranged from 17 to 39.5%. This system helped to accumulate high AMA values. Direct comparison with the literature data is impossible due to the novel nature of the proposed system. However, in the literature data, the EE in PLA nanospheres ranged from 19 to 30%, depending on the particle size (81 to 113 nm) [30]. The active substance release efficiency for both AMA and HEP showed high values reaching up to 47%. These values were much higher than those of the literature data, which allowed us to conclude that the proposed AMA/HEP/PPy system can be used for further studies in order to use it as a drug delivery system.

### 3.5. FTIR Analysis of AMA/HEP/PPy Films Before and After Release of AMA and HEP from the Polypyrrole Matrix

FTIR studies were performed to confirm the incorporation of AMA and HEP into the PPy matrix and after the desorption process, to determine the loss after the release process (Figure 6).

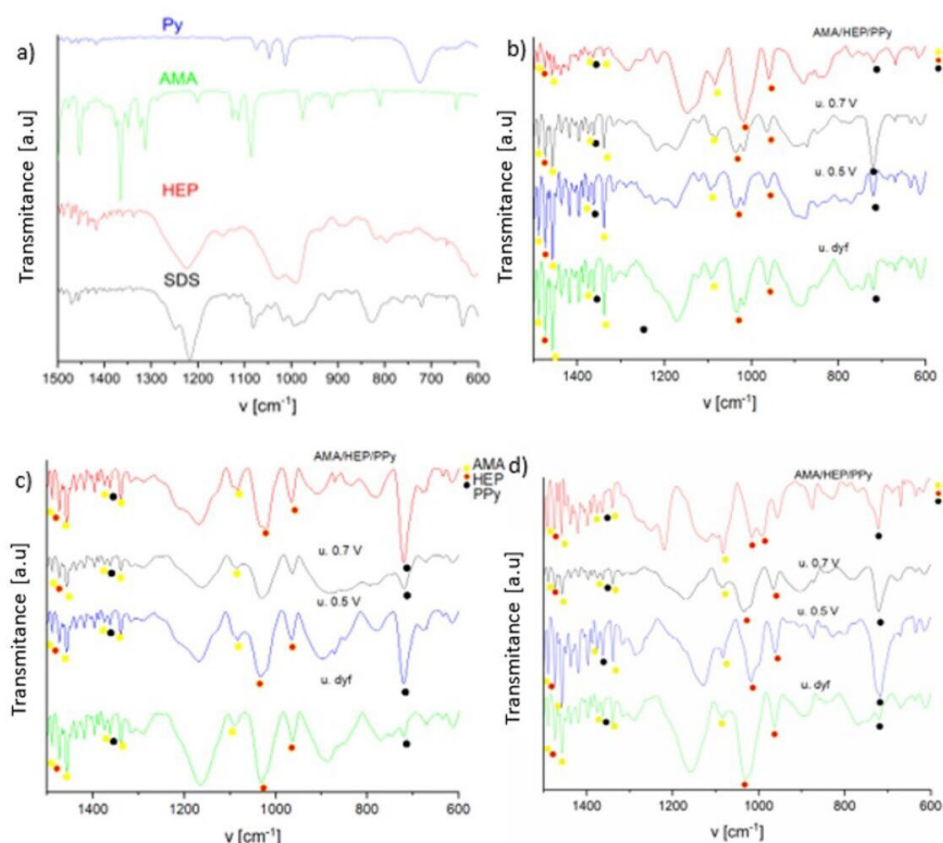


**Figure 6.** FTIR spectra of AMA/HEP/PPy films synthesized on ITO substrate: (a) Reference samples—blue line for pyrrole, green for amantadine, red for heparin, and black for sodium dodecyl sulfate; (b) film  $f_3$ ; (c)  $f_4$ ; (d)  $f_7$ , where (red line—synthesized film, black—film after 0.7 V release, blue—film after 0.5 V release, green—film after diffusion release) yellow dot—AMA, red—HEP, and black—PPy.

The results are shown in Figure 5. PPy-related bands were identified at  $1313\text{ cm}^{-1}$ , corresponding to the C-H in-plane deformation of PPy and N-H bending. Bands at  $1074\text{ cm}^{-1}$ ,  $1047\text{ cm}^{-1}$ ,  $1012\text{ cm}^{-1}$ , and  $811\text{ cm}^{-1}$ , attributed to the C-H wagging mode, along with a signal at  $727\text{ cm}^{-1}$  were also detected. Bands at  $1546$  and  $1452\text{ cm}^{-1}$  are associated with the fundamental vibration of the pyrrole ring, while the in-plane vibration of =C-H was observed at  $1298$  and  $1039\text{ cm}^{-1}$ . The vibration of the C-N bond corresponded to the band occurring at around  $1196\text{ cm}^{-1}$ . This analysis suggests a successful polymerization process resulting in PPy formation. Bands associated with HEP were detected at the following positions:  $1487\text{ cm}^{-1}$ , assigned to C=C stretching;  $1430\text{ cm}^{-1}$ , to the symmetric stretching of the carboxy group; and  $932\text{ cm}^{-1}$ , assigned to C-O-S stretching and C-O-C glycosidic bonds. The bands belonging to AMA were as follows:  $1455\text{ cm}^{-1}$ —band related to bending vibrations of N-H groups;  $1354\text{ cm}^{-1}$ —stretching vibrations of C-N bonds;  $1110\text{ cm}^{-1}$ ;  $974\text{ cm}^{-1}$  stretching vibrations of C-C bonds in the cycloalkyl ring [31]. The transmittance intensities of the  $1455\text{ cm}^{-1}$  band corresponding to AMA were compared for AMA/HEP/PPy coatings before and after the desorption process. These values are estimated and exemplary, and they refer to the spectrum recorded in the middle part of the sample. The band intensity is the highest for the synthesized films, and the lowest after release at 0.7 V. The changes in the band intensity are visible after the release of AMA and HEP from the polypyrrole matrix. The largest difference in transmittance before desorption to the band after release was detected for the band  $1455\text{ cm}^{-1}$  for  $f_4$  and  $f_7$  after stimulation with a potential of 0.7 V.

### 3.6. Long-Term Release of AMA and HEP from AMA/HEP/PPy Films

For the most promising systems, long-term release studies of drug substances were conducted (time scale of experiment: 48 h). The selection criterion was based on the possibility and effectiveness of providing a daily therapeutic dose, standardly used in the treatment of Alzheimer's disease. The studies were carried out according to the procedure described in Section 2.2. UV-Vis spectra of solutions during the release of drug substances from the films were recorded at a frequency of every 15 min for the first hour, every 20 min for the second hour, every 30 min during the third hour, every 60 min during 12 h, and every 240 min for the rest of the time. The spectra are presented in the figures below (Figure 7). Then, the cumulative release curves (CR—cumulative release) were prepared by plotting the relationship between the concentration of the drug released at time  $t$  and the total concentration of the solute (this value corresponds to the maximum concentration achieved during the release procedure from the matrix):  $\left(\frac{M_t}{M_\infty}\right) = f(t)$ . Selected mathematical models were fitted to the curves based on experimental data, which allowed for the description of the kinetics of the release of substances from the polymer network, including thin polymer films [32]. The mathematical models are summarized and briefly characterized in the table below (Table 6).

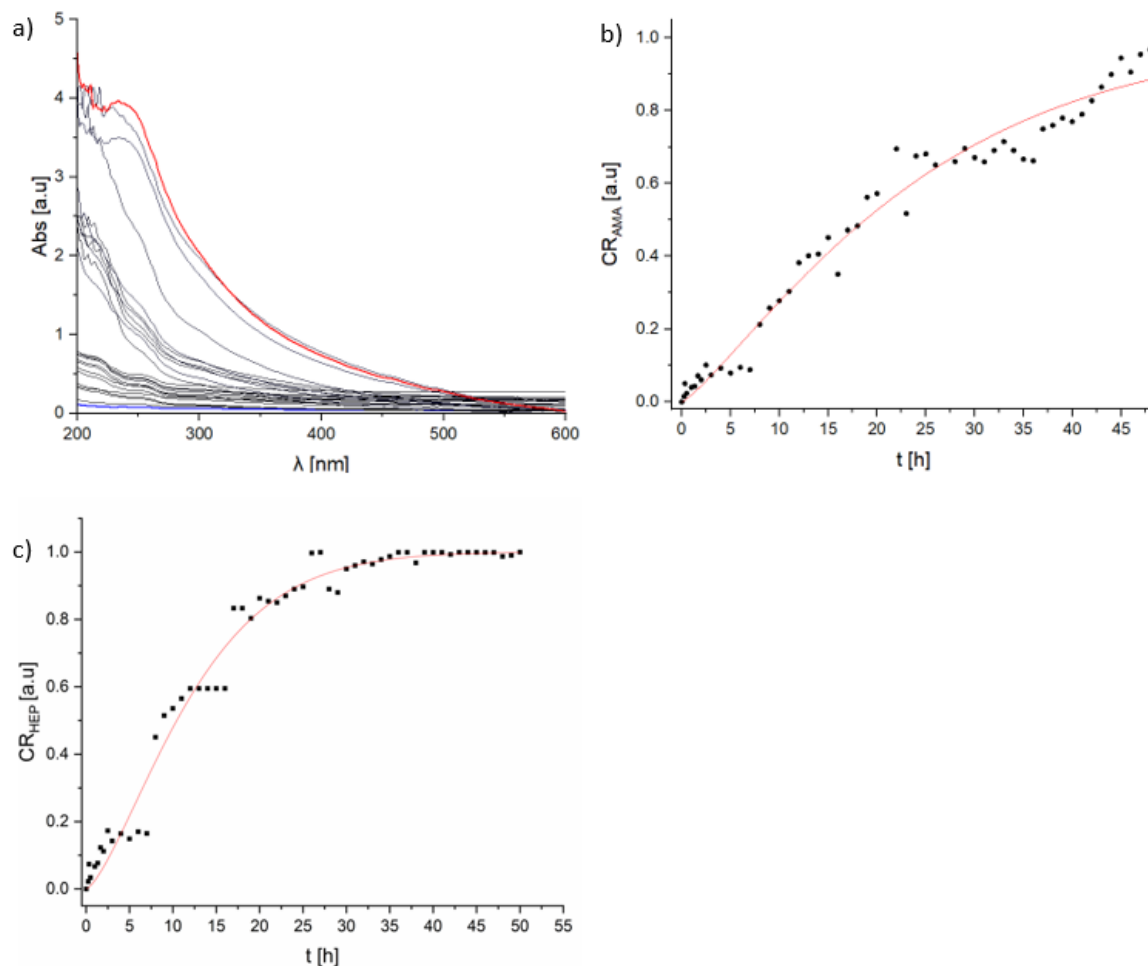


**Figure 7.** (a) UV-Vis spectrum of the solution during the release of AMA and HEP from the  $f_7$  film and the kinetic curves of the release of (b) AMA and (c) HEP with the simulation curve fitted by the Avrami model.

**Table 6.** Mathematical models describing controlled release kinetics.

Model	Analytical Relations	Description
Korsmeyer–Peppas (Power)	$\frac{M_t}{M_\infty} = k_p \cdot t^{n_p}$	$\frac{M_t}{M_\infty}$ is the fraction of drug released over time $t$ , $k_p$ is the Power release rate constant, and $n_p$ is the Power release exponent. The value of $n$ characterizes the drug release mechanism. To find the exponent $n$ , only part of the release curve was used, where $\frac{M_t}{M_\infty} < 0.6$ . If $n = 0.5$ , the release process is described as diffusion controlled, and if $n = 1$ , the process is non-Fick diffusion, and other controlling factors are present (e.g., swelling)
Avrami	$\frac{M_t}{M_\infty} = 1 - \exp(-k_A \cdot t^{n_A})$	$\frac{M_t}{M_\infty}$ is the fraction of drug released over time $t$ , $n_A$ is an Avrami parameter, and $k_A$ is the Avrami release rate constant. The value $n = 1$ indicates a first-order kinetic process (perturbed diffusion), and $n = 0.54$ corresponds to diffusive release kinetics

The first example of a mathematical model aimed to describe drug release from a matrix system was proposed by Higuchi [33]. Initially conceived for planar systems, it was then extended to different geometrics and porous systems [34]. The Avrami model was originally constructed to describe crystallization kinetics [35], but over time, it was adapted to simulate drug release from matrices. The value of  $n$  exponent estimates the type of release mechanism: a diffusion-controlled process for  $n$  between 0.5 and 1 with higher values indicating mechanisms involving swelling or degradation. Hence, it can provide insight into a mechanism of release process. The Avrami model is applicable for drug release simulation from a thin polymer matrix [36], especially for longer deposition times [37].

The UV-Vis spectra obtained for the  $f_7$  film were compared, and the concentration dependence curves for the active substance were plotted, on the basis of which analogous mathematical modeling was performed, which was the basis for the kinetic description of AMA and HEP from the AMA/HEP/PPy system (Figure 5).

AMA and HEP bands were identified, and absorbance values were recorded for the given wavelengths (Figure 7a). The release curves of AMA (Figure 7b). and HEP (Figure 7c). were plotted, for which 90% CR was achieved for AMA after 48 h, while for HEP, it was after 40 h. The best fit to the release curves was provided by the Avrami model. The calculated parameters of the tested models are listed in the table below (Table 7).

**Table 7.** Fitting parameters of AMA release kinetics curves obtained from mathematical simulations using the Avrami and Korsmeyer–Peppas models.

System	Film	Drug	Model		Avrami Fitted Parameters	
			R <sup>2</sup> (Avrami)	R <sup>2</sup> (K-P)	k	n
AMA/HEP/PPy (steel)	$f_3$	AMA	0.970	0.922	$0.019 \pm 0.036$	$0.973 \pm 0.057$
		HEP	0.981	0.969	$0.025 \pm 0.048$	$0.969 \pm 0.071$
AMA/HEP/PPy (ITO)	$f_7$	AMA	0.961	0.911	$0.017 \pm 0.029$	$0.961 \pm 0.054$
		HEP	0.975	0.911	$0.018 \pm 0.039$	$0.953 \pm 0.069$

The parameters'  $n$  values indicate that the release processes for both molecules are described by first-order kinetics. The minor differences between the  $k$  and  $n$  parameters were obtained for applied fitting models depending on substrate, and still higher values were noted for the  $f_3$  film on a steel substrate than that for the ITO one. It indicates a slightly more restricted release of molecules from the matrix of the samples deposited on the steel substrate. According to the literature, to obtain a therapeutic effect during the use of the drug, patients usually have to take AMA in daily doses of about 274 mg with the possibility of increasing to 400 mg [38,39]. The proposed systems could provide a dosage of 281 mg

per day (calculated based on 1 cm<sup>3</sup> of the deposited sample), covering part of the range of concentrations necessary to obtain therapeutic effects.

### 3.7. Microbiological Tests

In order to verify the possibility of using drug dosing systems in medical applications, the antibacterial activity of the steel plate surface was measured based on PN-EN ISO 22196:2007. The designations of the samples subjected to microbiological analysis are presented in the table below (Table 8).

**Table 8.** Designations of coatings used in microbiological tests.

Name	System	Parameter of Synthesis
BBT3 (f7)	AMA/HEP/PPy	E = 0.85 V, 20 c
BBT4 (f7)	AMA/HEP/PPy	
A control	steel substrate 316l	-
B control	steel substrate 316l	-

A slight reduction of microorganisms around the materials contacted with the Gram-negative strain occurs in the area of the BBT4 material (marked as 4). However, due to the lack of a homogeneous area, no growth inhibition zone was determined for it. The material (BBT3) contacted with the Gram-positive strain *Staphylococcus aureus* (*S. aureus*) shows a growth inhibition zone after 24 h of incubation. The size of the inhibition zones is presented in the figure (Figure 8), and it was equal to 7 mm according to *S. aureus*.

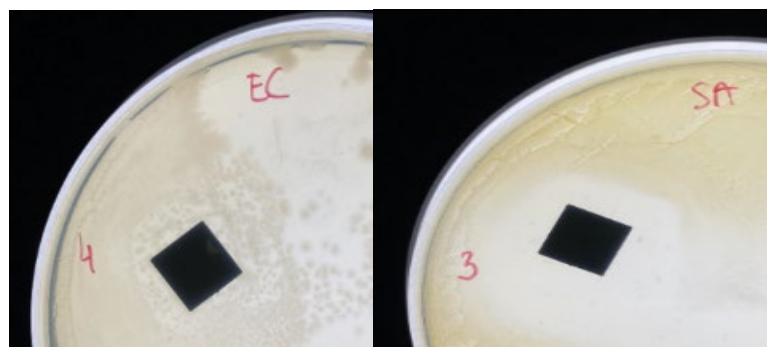


**Figure 8.** Growth inhibition zone visible around the tested materials on agar media (MHA) after 24 h of bacterial culturing with *Escherichia coli* (*E. coli* EC) and *S. aureus* (SA).

Antimicrobial activity for *S. aureus*: The degree of reduction was determined for the BBT3 material. The obtained results indicate that the materials have a biocidal effect. The reference material (B) did not show any biocidal properties. The data obtained during the experiment are summarized in Figure 9.

The degrees of reduction of *S. aureus* and *E. coli* bacteria after 24 h of contact of the tested materials with microorganisms were equal to 71.42% (reduction log 1.48) for *E. coli* and 93.94% (reduction log 4.13) for *S. aureus*.

The antibacterial properties of the BBT3 material allows it to be considered as a material with antibacterial potential in the presence of the *S. aureus* strain, with reduction ratio indices above 2 (BBT3). The percentage reduction ratio indicates a 90–100% reduction of bacteria in the suspension.

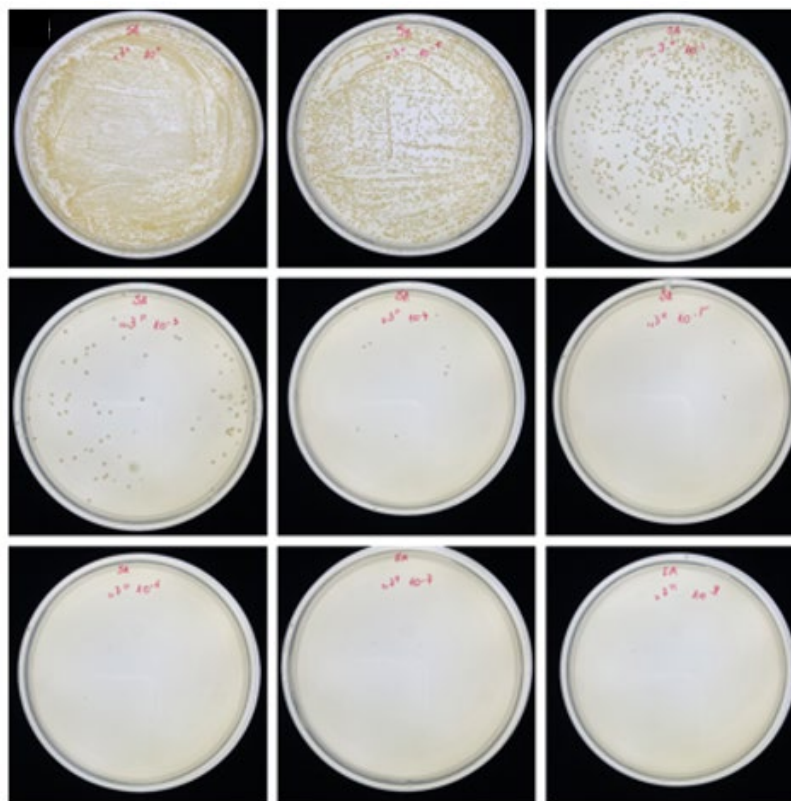


**Figure 9.** Inoculation of *S.aureus* on PCA medium; reading 24 h after inoculation on the tested material BBT3.

#### 4. Discussion

The increase of the potential window during synthesis and the number of cycles influenced the increase of the layer thickness. The most effective polymerization process and electrochemical stability of the coatings were visible for  $f_7$ . Increasing the potential window during synthesis influenced the increase of the process and electrochemical stability of the obtained coatings on both substrates. After the release of AMA and HEP, single globular structures with a diameter of  $0.05 \mu\text{m}$  were visible. AMA increased the adhesion of the coating to the ITO substrate. The results indicate a significantly better adhesion for the films on the steel substrate. The  $f_7$  film showed the best adhesion, as only small flakes of the coating were detached at the intersections of the lines (less than 5% of the area). The  $f_5$  coating detached in 15% of the area of the incision grid and  $f_6$  from the area of 30%. The release efficiency of the active substance for both AMA and HEP showed high values reaching even 47%. These values were much higher than those of the literature data, which allowed us to conclude that the proposed AMA/HEP/PPy system can be used for further studies on its use as a drug delivery system.

#### 5. Conclusions

AMA and HEP were successfully incorporated into the PPy matrix. The films deposited on the steel substrate showed a compact, smooth structure, where there were no visible organized structures. After release, the film became corrugated. AMA-added films improved the adhesion of the coating to the ITO substrate. The  $f_7$  film showed the best adhesion, with only small flakes peeling off at the line intersections (less than 5% of the area). The short-term release of AMA and HEP showed promising results for film  $f_7$ . Based on short-term results, long-term tests were conducted. For the AMA/HEP/PPy system, the most effective film in terms of drug release from the matrix (based on short-term release studies) was selected for the steel and ITO substrates, and release curves were plotted. The best fit of the experimental curves was obtained using the Avrami model. The curves



showed an n-factor above 0.54, indicating first-order release kinetics with a significant matrix effect on this process. DDS released the drug at a constant rate, thus maintaining the drug concentration in the therapeutic window for a longer period. The release curves indicate a 95% efficiency of AMA release over the studied time period and protocol. The proposed system was able to provide a daily dose that ensures a therapeutic effect. This was a significant step towards developing systems capable of delivering a wider range of doses, potentially in line with the full spectrum recommended for therapeutic efficacy. The antibacterial properties of the material can be considered as a composite with antibacterial potential in the presence of the *S. aureus* strain. The percentage reduction ratio indicates a 90–100% reduction of bacteria in the suspension.

## 6. Patents

Research based on the databases developed from the patent application: Kulik S., Golba S., Stodolak Zych E., Kurpanik R., Polymer composite based on polypyrrole, implant with a coating of a polymer composite based on polypyrrole and a method of manufacturing an implant with a coating of a polymer composite based on polypyrrole. Application data: 17 September 2024. Confirmed number: P.449842.

**Supplementary Materials:** The following supporting information can be downloaded at: <https://www.mdpi.com/article/10.3390/coatings14111389/s1>, Figure S1: Synthesis of AMA/HEP/PPy in 0.1 M SDS: (a) f1; (b) f5; (c) f2; (d) f6. Figure S2: Cyclic voltammogram of AMA/HEP/PPy films in doping/dedoping state of: (a) f1; (b) f5; (c) f2; (d) f6. Figure S3: SEM images of the film f7 AMA/HEP/PPy on steel substrate: (a,c) before AMA and HEP release; (b,d) after 0.7 V potential release of AMA and HEP. Figure S4: Adhesion test of AMA/HEP/PPy films before and after the adhesion test: on ITO substrate (a) f1; (b) f2; (c) f3; (d) f4; (e) f5; (f) f6; (g) f7; (h) f8.

**Author Contributions:** Conceptualization, S.K., S.G. and R.K.; data curation, S.K. and E.S.-Z.; formal analysis, S.K., S.G., I.M., E.S.-Z. and R.K.; funding acquisition, S.K. and S.G.; investigation, S.K., S.G., I.M., E.S.-Z. and R.K.; methodology, S.K. and E.S.-Z.; project administration, S.K. and S.G.; resources, S.K. and S.G.; software, S.K.; supervision, S.G., E.S.-Z. and R.K.; validation, S.K., S.G. and E.S.-Z.; visualization, S.K.; writing—original draft, S.K.; writing—review & editing, S.G. All authors have read and agreed to the published version of the manuscript.

**Funding:** The research was funded by the Doctoral School of the University of Silesia in Katowice Research Excellence Initiative (IDB) of the UŚ and the “Freedom of Research” competition—3rd edition of IDB, UŚ.

**Institutional Review Board Statement:** Not applicable.

**Informed Consent Statement:** Not applicable.

**Data Availability Statement:** Dataset available on request from the authors.

**Conflicts of Interest:** The authors declare no conflicts of interest.

## References

1. World Health Organization. Available online: [https://www.who.int/health-topics/ageing#tab=tab\\_1](https://www.who.int/health-topics/ageing#tab=tab_1) (accessed on 16 June 2024).
2. United Nations. Available online: <https://www.un.org/development/desa/pd/content/world-population-ageing-2017-highlightsasp> (accessed on 16 June 2024).
3. Klimova, B.; Kuca, K. Speech and language impairments in dementia. *J. Appl. Biomed.* **2016**, *14*, 97–103. [CrossRef]
4. Klimova, B.; Maresova, P.; Valis, M.; Hort, J.; Kuca, K. Alzheimer’s disease and language impairments: Social intervention and medical treatment. *Clin. Interv. Aging* **2015**, *10*, 1401–1407. [CrossRef]
5. Maresova, P.; Hruska, J.; Klimova, B.; Barakovic, S.; Krejcar, O. Activities of Daily Living and Associated Costs in the Most Widespread Neurodegenerative Diseases: A Systematic Review. *Clin. Interv. Aging* **2020**, *15*, 1841–1862. [CrossRef]
6. Fomo, G.; Waryo, T.; Feleni, U.; Baker, P.; Iwuoha, E. Electrochemical Polymerization. In *Functional Polymers—Polymers and Polymeric Composites: A Reference Series*; Jafar Mazumder, M., Sheardown, H., Al-Ahmed, A., Eds.; Springer: Berlin/Heidelberg, Germany, 2019; pp. 105–131. [CrossRef]
7. Skovronsky, D.M.; Lee, V.M.-Y.; Trojanowski, J.Q. Neurodegenerative Diseases: New Concepts of Pathogenesis and Their Therapeutic Implications. *Annu. Rev. Pathol. Mech. Dis.* **2006**, *1*, 151–170. [CrossRef]

8. Schmidt, M.L.; Zhukareva, V.; Newell, K.L.; Lee, V.M.; Trojanowski, J.Q. Tau isoform profile and phosphorylation state in dementia pugilistica recapitulate Alzheimer's disease. *Acta Neuropathol.* **2000**, *101*, 518–524. [CrossRef]
9. Akhtar, A.; Andleeb, A.; Waris, T.S.; Bazzar, M.; Moradi, A.-R.; Awan, N.R.; Yar, M. Neurodegenerative diseases and effective drug delivery: A review of challenges and novel therapeutics. *J. Control. Release* **2020**, *10*, 1152–1167. [CrossRef]
10. Metman, L.V.; Del Dotto, P.; van den Munckhof, P.; Fang, J.; Mouradian, M.M.; Chase, T.N. Amantadine as treatment for dyskinesias and motor fluctuations in Parkinson's disease. *Neurology* **1998**, *50*, 1323–1326. [CrossRef]
11. Jain, K.K. Drug Delivery Systems—An Overview. *Methods Mol. Biol.* **2008**, *437*, 1–50. [CrossRef]
12. Smela, E. Conjugated polymer actuators for biomedical applications. *Adv. Mater.* **2003**, *15*, 481–494. [CrossRef]
13. Ferraz, N.; Strømme, M.; Fellström, B.; Pradhan, S.; Nyholm, L.; Mihranyan, A. In vitro and in vivo toxicity of rinsed and aged nanocellulose–polypyrrole composites. *J. Biomed. Mater. Res.* **2012**, *100*, 2128–2138. [CrossRef]
14. Kamalesh, S.; Tan, P.; Wang, J.; Lee, T.; Kang, E.-T.; Wang, C.-H. Biocompatibility of electroactive polymers in tissues. *J. Biomed. Mater. Res.* **2000**, *52*, 467–478. [CrossRef]
15. Kontturi, K.; Pentti, P.; Sundholm, G. Polypyrrole as a model membrane for drug delivery. *J. Electroanal. Chem.* **1998**, *453*, 231–238. [CrossRef]
16. Gandhi, M.R.; Murray, P.; Spinks, G.M.; Wallace, G.G. Mechanism of electromechanical actuation in polypyrrole. *Synth. Met.* **1995**, *73*, 247–256. [CrossRef]
17. Svirskis, D.; Travas-Sejdic, J.; Rodgers, A.; Garg, S. Electrochemically controlled drug delivery based on intrinsically conducting polymers. *J. Control. Release* **2010**, *146*, 6–15. [CrossRef]
18. Shah, S.A.A.; Firlak, M.; Berrow, S.R.; Halcovitch, N.R.; Baldock, S.J.; Yousafzai, B.M.; Hathout, R.M.; Hardy, J.G. Electrochemically Enhanced Drug Delivery Using Polypyrrole Films. *Materials* **2018**, *11*, 1123. [CrossRef]
19. Alshammary, B.; Walsh, F.C.; Herrasti, P. Electrodeposited conductive polymers for controlled drug release: Polypyrrole. *J. Solid State Electrochem.* **2016**, *20*, 839–859. [CrossRef]
20. Hasan, N.; Bhuyan, M.M.; Jeong, J.-H. Single/Multi-Network Conductive Hydrogels—A Review. *Polymers* **2024**, *16*, 2030. [CrossRef]
21. Wang, X.; Li, X.; Zhao, L.; Li, M.; Li, Y.; Yang, W. Polypyrrole-doped conductive self-healing multifunctional composite hydrogels with a dual crosslinked network, The Royal Society of Chemistry. *Soft. Matter.* **2021**, *17*, 8363–8372. [CrossRef]
22. Hazarika, J.; Kumar, A. Controllable synthesis and characterization of polypyrrole nanoparticles in sodium dodecylsulphate (SDS) micellar solution. *Synth. Met.* **2013**, *175*, 155–162. [CrossRef]
23. Kirschbaum, J. Amantadine. *Anal. Profiles Drug Subst.* **1983**, *12*, 1–36. [CrossRef]
24. Rodríguez-Torres, M.; Díaz-Torres, L.; Romero-Servin, S. Heparin Assisted Photochemical Synthesis of Gold Nanoparticles and Their Performance as SERS Substrates. *Int. J. Mol. Sci.* **2014**, *15*, 19239–19252. [CrossRef]
25. Shama, S.A.; Amin, A.S.; Mabrouk, E.S.M.; Omara, H.A. Utility of oxidation–reduction reaction for the spectrophotometric determination of amlodipine besylate. *Arab. J. Chem.* **2009**, *2*, 59–63. [CrossRef]
26. Ryan, E.M.; Breslin, C.B. Formation of polypyrrole with dexamethasone as a dopant: Its cation and anion exchange properties. *J. Electroanal. Chem.* **2018**, *824*, 188–194. [CrossRef]
27. Arroyoa, J.; Akieh-Pirkanniemi, M.; Lisakb, G.; Latonena, R.M.; Bobacka, J. Electrochemically controlled transport of anions across polypyrrole-based membranes. *J. Membr. Sci.* **2019**, *581*, 50–57. [CrossRef]
28. Song, Y.; Wei, J.; Ma, Y.; Zeng, P.; Kong, M. Removal and recovery of amantadine from water by liquid–liquid extraction. *Environ. Earth Sci.* **2015**, *73*, 4931–4938. [CrossRef]
29. Mazibuko, Z.; Indermun, S.; Govender, M.; Kumar, P.; Du Toit, L.C.; Choonara, Y.E.; Pillay, V. Targeted Delivery of Amantadine-loaded Methacrylate Nanosphere-ligands for the Potential Treatment of Amyotrophic Lateral Sclerosis. *J. Pharm. Pharm. Sci.* **2018**, *21*, 94. [CrossRef]
30. Rivas, L.; Sánchez-Cortés, S.; Stanicova, J.; García-Ramos, J.; Miskovsky, P. FT-Raman, FTIR and surface-enhanced Raman spectroscopy of the antiviral and antiparkinsonian drug amantadine. *Vib. Spectrosc.* **1999**, *20*, 179–188. [CrossRef]
31. Wang, L.-Y.; Zhao, M.-Y.; Bu, F.-Z.; Niu, Y.-Y.; Yu, Y.-M.; Li, Y.-T.; Wu, Z.-Y. Cocrystallization of Amantadine Hydrochloride with Resveratrol: The First Drug–Nutraceutical Cocrystal Displaying Synergistic Antiviral Activity. *Cryst. Growth Des.* **2021**, *21*, 2763–2776. [CrossRef]
32. Suman Kumar Valeveti, Shailaja Pashikanti Design, development, and evaluation of transdermal patches containing memantine hydrochloride. *J. Appl. Pharm.* **2023**, *15*, 5. [CrossRef]
33. Higuchi, T.J. Mechanism of sustained medication. Theoretical analysis of rate of release of solid drugs dispersed in solid matrices. *Pharm. Sci.* **1963**, *84*, 1464–1477. [CrossRef]
34. Grassi, M.; Grassi, G. Mathematical modeling and controlled drug delivery: Matrix systems. *Curr. Drug Deliv.* **2005**, *2*, 97–116. [CrossRef] [PubMed]
35. Avrami, M. Kinetics of Phase Change. I General Theory. *J. Chem. Phys.* **1939**, *7*, 1103–1112. [CrossRef]
36. Brady, Á.; Sakathinatan, I.; Barreca, D.; Maccato, C.; McCormac, T. Electrochemical Doping and Surface Studies of Poly(3,4-Ethylenedioxythiophene) Films for the Release of the Anticancer Drug Mitoxantrone. Available online: [https://www.researchgate.net/publication/373428270\\_Electrochemical\\_Doping\\_and\\_Surface\\_Studies\\_of\\_Poly34-Ethylenedioxythiophene\\_Films\\_for\\_the\\_Release\\_of\\_the\\_Anticancer\\_Drug\\_Mitoxantrone](https://www.researchgate.net/publication/373428270_Electrochemical_Doping_and_Surface_Studies_of_Poly34-Ethylenedioxythiophene_Films_for_the_Release_of_the_Anticancer_Drug_Mitoxantrone) (accessed on 1 September 2024). [CrossRef]

37. Alizadeh, N.; Shamaeli, E. Electrochemically controlled release of anticancer drug methotrexate using nanostructured polypyrrole modified with cetylpyridinium: Release kinetics investigation. *Electrochim. Acta* **2014**, *130*, 488–496. [CrossRef]
38. Drugs.com. Amantadine Dosage. 2023. Available online: [https://www.drugs.com/dosage/amantadine.html#Usual\\_Adult\\_Dose\\_for\\_Parkinson\\_s\\_Disease](https://www.drugs.com/dosage/amantadine.html#Usual_Adult_Dose_for_Parkinson_s_Disease) (accessed on 1 September 2024).
39. Mayo Clinic. Amantadine (Oral Route). 2024. Available online: <https://www.mayoclinic.org/drugs-supplements/amantadine-oral-route/proper-use/drg-20061695> (accessed on 1 September 2024).

**Disclaimer/Publisher’s Note:** The statements, opinions and data contained in all publications are solely those of the individual author(s) and contributor(s) and not of MDPI and/or the editor(s). MDPI and/or the editor(s) disclaim responsibility for any injury to people or property resulting from any ideas, methods, instructions or products referred to in the content.